

pubs.acs.org/JACS Article

# Ring-and-Lock Interactions in Self-Healable Styrenic Copolymers

Samruddhi Gaikwad and Marek W. Urban\*



Cite This: https://doi.org/10.1021/jacs.3c01199



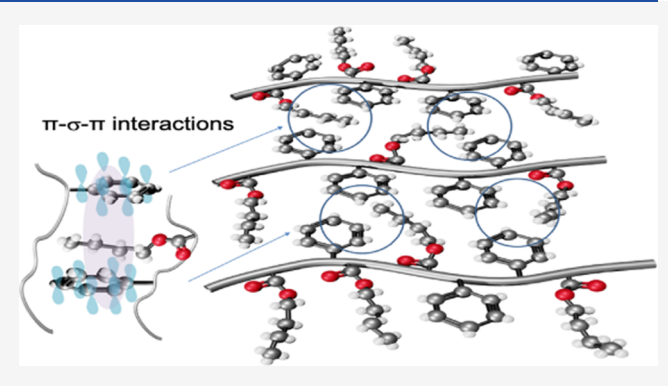
**ACCESS** I

III Metrics & More

Article Recommendations

SI Supporting Information

**ABSTRACT:** Commodity copolymers offer many useful applications, and their durability is critical in maintaining desired functions and retaining sustainability. These studies show that primarily alternating styrene/n-butyl acrylate [p(Sty/nBA)] copolymers self-heal without external intervention when monomer molar ratios are within the 45:55-53:47 range. This behavior is attributed to the favorable interchain interactions between aliphatic nBA side groups being sandwiched by aromatic rings forming ring-and-lock associations driven by pi-sigma-pi ( $\pi$ - $\sigma$ - $\pi$ ) interactions. Guided by molecular dynamics (MD) simulations combined with spectroscopic and thermomechanical analysis, the ring-and-lock interchain van der Waals forces between  $\pi$  orbitals of aromatic rings and sigma components of aliphatic side groups are



responsible for self-healing. Despite the frequent occurrence of these interactions in biological systems (proteins, nucleic acids, lipids, and polysaccharides), these largely unexplored weak and ubiquitous molecular forces between the soft acid aliphatic and soft base aromatic electrons may be valuable assets in the development of polymeric materials with sustainable properties.

# ■ INTRODUCTION

Styrene-based copolymers represent a significant commodity market share of overall polymer technologies with a diverse spectrum of properties and applications ranging from pressuresensitive adhesives to cosmetics, packaging products, or building materials, to name just a few. These copolymers can be readily produced, offering exceptional hydrophobic properties with copolymer-composition-controlled tunable elasticity and hardness. Although the ability to copolymerize styrene (Sty) with n-butyl acrylate (nBA) and other monomers with variable monomer molar ratios provides an opportunity for creating stiff-to-flexible products with useful optical features, 1 these materials are not exempted from damage and degradation. Although theoretical predictions suggested that the degradation of a Sty molecule has a negligible effect on the formation of ozone in the troposphere, experimental studies have challenged these conclusions by showing that Sty oxidation reactions may lead to the formation of significant amounts of formaldehyde and benzaldehyde, thus meaningfully contributing to secondary organic aerosols (SOAs).3 Owing to thermomechanical degradation, copolymerized styrene may produce monomers, dimers, and trimers through chain scission, followed by  $\beta$ -scission manifested by a loss of mechanical properties. Embedding self-healing to alleviate plastic pollution and minimize disposal is economically and environmentally beneficial to enhance sustainability, retain useful functions, and avoid catastrophic failure of Sty-based copolymers. An ultimate goal is to create "long-lived" synthetic copolymers resistant to unintended loss of functions.

The last couple of decades witnessed the development of diversified physical and/or chemical approaches that have led to self-healing polymeric materials.<sup>4</sup> Ranging from covalent bond reformation,<sup>5-7</sup> dynamic supramolecular chemistry Hbonding,<sup>8,9</sup> coordination chemistries,<sup>10</sup> van der Waals (vdW)<sup>11</sup> and ionic interactions, 12 encapsulation of reactive compounds, 13 incorporations of superparamagnetic nanoparticles, 14 to copolymerization of ionic liquids 15 are just a few examples that resulted in the development of this attractive class of materials. Although the quest for economically feasible self-healing polymer technologies continues, of particular interest is self-healing by ubiquitous vdW-driven inter- and intrachain interactions without the need of elaborate chemical modifications. In spite of somewhat unfavorable methyl methacrylate (MA) and n-butyl acrylate (nBA) reactivity ratios ( $r_{\text{Ma}}$ = 1.75–3.15 and  $r_{n\text{BA}}$ = 0.2–0.39), self-healing in the 45:55 to 50:50 MMA/nBA monomer molar ratio range was achieved in predominantly alternating/random poly(methyl methacrylate/n-butyl acrylate) [p(MMA/nBA)] copolymers through key-and-lock interactions. 11 Taking this step further and embedding rebondable chemical cross-links, reprocessable self-healable thermosets were developed. 16,17 These reactivity

Received: February 1, 2023 Published: April 17, 2023



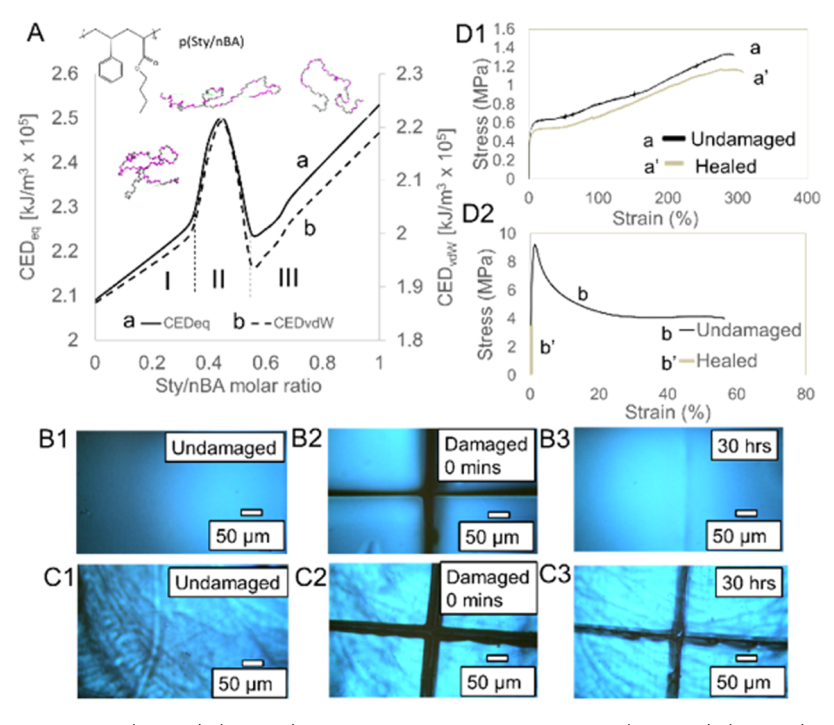


Figure 1. (A) Cohesive energy densities ( $\text{CED}_{\text{eq}}$ ) (curve a) and vdW contributions to  $\text{CED}_{\text{eq}}$  ( $\text{CED}_{\text{vdW}}$ ) (curve b) plotted as a function of Sty % molar content in p(Sty/nBA) copolymers; average end-to-end distances ( $r_{\text{eq}}$ ) for 40:60 (I), 47:53 (II), and 60:40 (III) p(Sty/nBA) compositions extracted from MD simulations ( $r_{\text{eq}} = 23.5$ , 38.7, and 30.6 Å, respectively). (B) Optical images of undamaged (B1), damaged (B2), and 30 h after damage (B3) 47:53 p(Sty/nBA) copolymers. (C) Optical images of undamaged (C1), damaged (C2), and 30 h after damage (C3) 60:40 p(Sty/nBA) copolymers. (D) Stress—strain curves for 47:53 (D1) and 60:40 (D2) p(Sty/nBA) copolymers; a/a' and b/b' curves represent undamaged and self-healed copolymers, respectively.

ratio differences, even for reversible deactivation radical copolymerizations, <sup>18</sup> will not generate purely alternating topologies <sup>19</sup> unless bulky groups such as 2-ethylfenchyl methacrylate (EFMA) are used. <sup>20</sup> These electronic effects offered by large electron density groups such as styrene will generate primarily alternating copolymers. This is reflected in the reactivity ratios of styrene (Sty) and n-butyl acrylate (nBA) ( $r_s = 0.88$  and  $r_b = 0.22$ , 21 and  $r_s \times r_n = 0.19$ ), which favors alternating topologies even under statistical copolymerization conditions. Driven by the hypothesis that predominantly alternating copolymer topologies favor self-healing, the question is if the copolymerization of Sty, known for ring-ring interactions facilitated by  $\pi$  orbitals, with nBA to form p(Sty/nBA) (Figure 1) exhibits autonomous self-healing, and if so, what molecular processes govern this behavior?

## RESULTS AND DISCUSSION

To initially validate the hypothesis that the primary forces for self-healing are enhanced dipolar inter- and/or intrachain interactions typically reflected in composition-dependent higher cohesive energy densities, molecular dynamics (MD) simulations were employed to estimate cohesive energy densities (CED<sub>eq</sub>) and vdW contributions (CED<sub>vdw</sub>) to the CED<sub>eq</sub> values as a function of the copolymer molar ratio in p(Sty/nBA). Figure 1A illustrates CED<sub>eq</sub> (curve a) as well as CED<sub>vdW</sub> (curve b) values as a function of the copolymer composition. Both curves exhibit the maxima at 2.5  $\times$  10<sup>5</sup> kJ/m $^3$  CED<sub>eq</sub> in the 45:55–53:47 Sty/nBA monomer molar range, suggesting that copolymers in this compositional range will likely self-heal. The dominating copolymer conformations shown in Figure 1A extracted from MD simulations for 40:60 p(Sty/nBA) (I), 47:53 p(Sty/nBA) (II), and 60:40

p(Sty/nBA) (III) monomer molar ratio ranges may exhibit extended helix conformations with an average value of the end-to-end distance of  $r_{\rm eq} = \sim 38.7$  Å for 47:53 p(Sty/nBA) copolymer chains (II), whereas outside this molar ratio range [40:60 (I) and 60:40 p(Sty/nBA) (III)], the chains adapt globular morphologies with the  $r_{\rm eq}$  values of 23.6 Å (I) and 30.6 Å (III), respectively.

Guided by MD simulations, we copolymerized a series of p(Sty/nBA) copolymers with the molar ratios of 40:60, 47:53, and 60:40 (determined by <sup>1</sup>H NMR, Figures S1-S3) and examined their self-healing properties. While the Supporting Information provides experimental details and copolymer properties (Figures S4-S6 and Tables S1-S5), optical images of undamaged (Figure 1B1), damaged (Figure 1B2), and selfhealed (Figure 1B3) films with the 47:53 Sty/nBA molar ratios show that self-healing occurs, whereas 60:40 p(Sty/nBA) films do not self-heal even after extended periods of time (Figure 1C1-C3) (40:60 Sty/nBA films are too soft and flow due to low  $T_g = -0.5$  °C; Figure S6). To examine the recovery of mechanical properties, Figure 1D1 illustrates stress-strain curves for undamaged (curve a) and self-healed (curve a') 47:53 p(Sty/nBA) copolymers. Young's modulus (E) of the undamaged copolymer is 52.2 ± 7.5 MPa, which upon a damage-repair cycle recovers 98% (±10%) of initial stress and 83% ( $\pm$  2%) strain values. The same tensile experiments conducted on non-self-healable 60:40 p(Sty/nBA) copolymers (Figure 1D2, curves b and b') exhibit 33% ( $\pm 2.5\%$ ) of initial tensile stress and 9.5% ( $\pm 11\%$ ) of strain recoveries. Block p(Sty-b-nBA) copolymers (Figures S7–S10) with a molar ratio of 47:53 also do not self-heal (Figure S11).

The presence of aromatic rings raises the question of the contributions to the self-healing of  $\pi$  orbitals and interactions

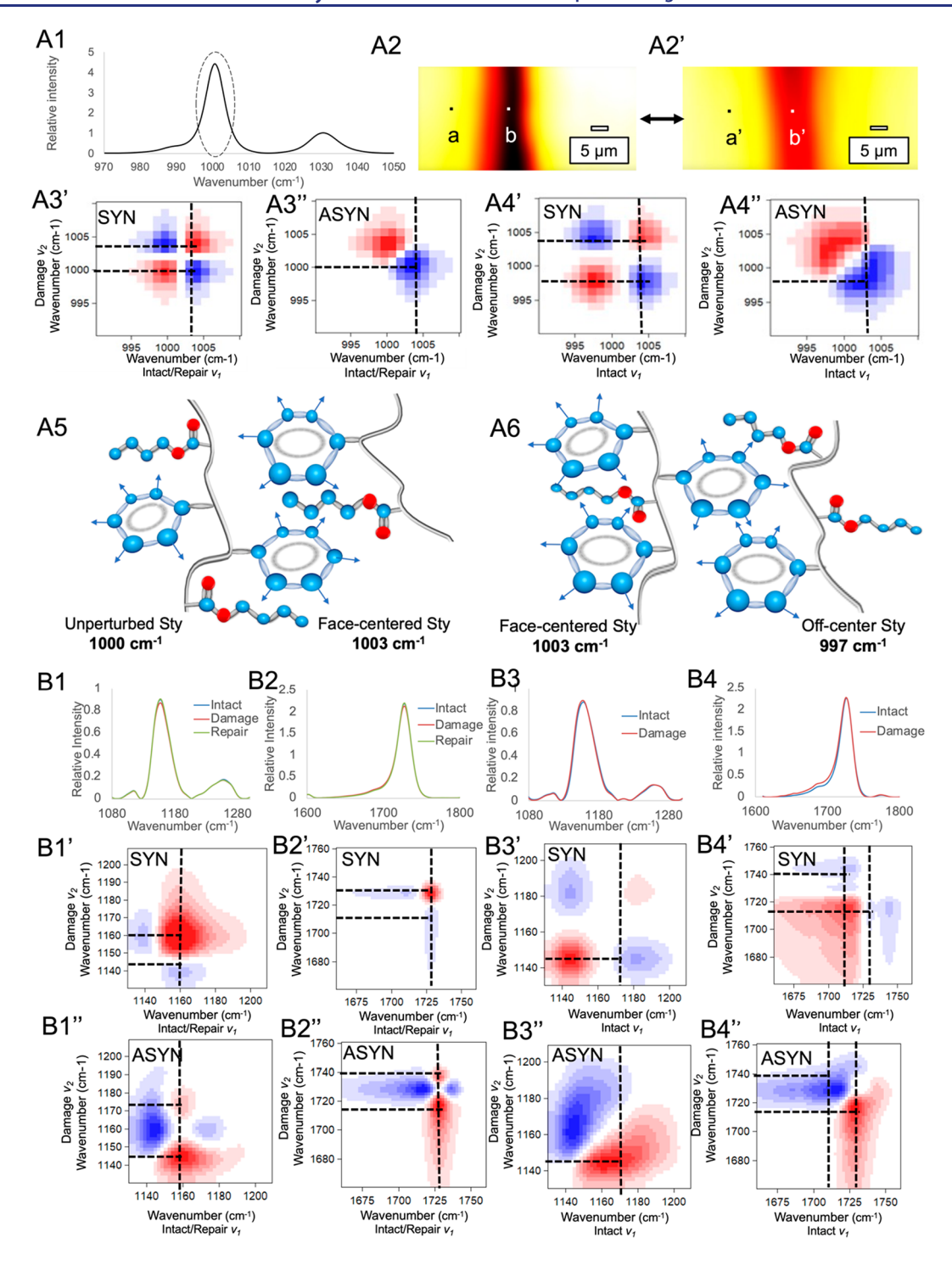
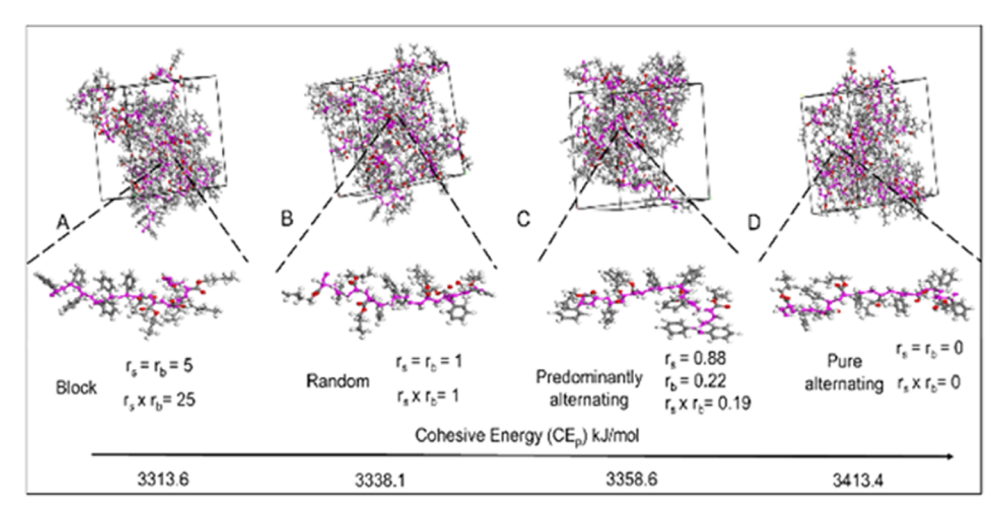


Figure 2. (A1) Raman spectrum of 47:53 p(Sty/nBA) copolymers (highlighted "---" band at 1000 cm<sup>-1</sup> due to the C–C ring breathing mode). (A2) Raman imaging of p(Sty/nBA): a, intact region and b, inside cut (black) region. (A2') Raman imaging of self-healed p(Sty/nBA): a', intact region and b', self-healed (red) region. (A3') SYN 2D-COS of damage (ν<sub>2</sub>) vs intact (ν<sub>1</sub>) 47:53 p(Sty/nBA) copolymer. (A3") ASYN 2D-COS of damage (ν<sub>2</sub>) vs intact (ν<sub>1</sub>) of 60:40 p(Sty/nBA) copolymer. (A4") ASYN 2D-COS of damage (ν<sub>2</sub>) vs intact (ν<sub>1</sub>) of 60:40 p(Sty/nBA) copolymer. (A4") ASYN 2D-COS of damage (ν<sub>2</sub>) vs intact (ν<sub>1</sub>) of 60:40 p(Sty/nBA) copolymer. (A4") ASYN 2D-COS of damage (ν<sub>2</sub>) vs intact (ν<sub>1</sub>) of 60:40 p(Sty/nBA) copolymer. (A5) Schematic representation of ring—ring interactions in self-healable 47:53 p(Sty/nBA) copolymers and corresponding breathing vibrations observed in Raman spectra. (A6) Schematic representation of ring—ring interactions in non-self-healable 60:40 p(Sty/nBA) copolymers and corresponding breathing vibrations observed in Raman spectra. FTIR spectra were collected from intact, damaged, and repaired areas of 47:53 p(Sty/nBA) copolymer (B1) in the C–O–C (1158 cm<sup>-1</sup>) and (B2) C=O stretching (1728 cm<sup>-1</sup>) regions. FTIR spectra of the 47:53 p(Sty/nBA) copolymer collected from intact and damaged areas of the 60:40 p(Sty/nBA) copolymer (B3) in the C–O–C (1158 cm<sup>-1</sup>) and (B4) C=O stretching (1728 cm<sup>-1</sup>) regions. (B1') SYN and (B1") ASYN 2D-COS of damage (ν<sub>2</sub>) vs intact (ν<sub>1</sub>) in the C–O–C (1158 cm<sup>-1</sup>) region. (B2') SYN and (B2") ASYN 2D-COS of damage (ν<sub>2</sub>) vs intact (ν<sub>1</sub>) in the C=O stretching (1728 cm<sup>-1</sup>) region. FTIR spectra of the 60:40 p(Sty/nBA) copolymer: (B3') SYN and (B3") ASYN 2D-COS of damage (ν<sub>2</sub>) vs intact (ν<sub>1</sub>) in the C=O stretching (1728 cm<sup>-1</sup>) region. (B4') SYN and (B4") ASYN 2D-COS of damage (ν<sub>2</sub>) vs intact (ν<sub>1</sub>) in the C=O stretching (1728 cm<sup>-1</sup>) region.



**Figure 3.** (A–D) MD simulations of model Sty/nBA copolymers with the following reactivity ratios: (A)  $r_s = r_b = 5$ ; (B)  $r_s = r_b = 1$ ; (C)  $r_s = 0.88$  and  $r_b = 0.22$  (experimental values<sup>21</sup>); and (D)  $r_s = r_b = 0$ .

with aliphatic side groups. The primary events differentiating damaged and undamaged/self-healed states are vibrational band intensity changes detected by Raman and Fourier transform infrared (FTIR) imaging. <sup>22</sup> Figure 2A1 illustrates the one-dimensional Raman spectrum collected from point a (Figure 2A2) of the 47:53 p(Sty/nBA) copolymer where the C-C breathing mode intensity of the Sty ring at 1000 cm<sup>-1</sup> (Figure 2A1; dashed circle) is detected. Raman spectra collected from damaged (Figure 2A2, point b) and repaired areas (Figure 2A2', points a'/b') show visually undistinguishable intensity changes upon the damage-repair cycle, which can be resolved by two-dimensional correlation spectroscopic  $(2D\text{-}COS)^{23}$  analysis. This approach enables the correlation between spectra collected from damaged (Y-axis) and intact/ repaired (X-axis) areas by measuring synchronous (SYN) and asynchronous (ASYN) responses (Tables S6-S7). 2D-COS analysis of intact/repaired and damaged copolymers in the 990-1010 cm<sup>-1</sup> region of SYN spectra (Figure 2A3') shows two Raman cross-peaks at 1003 and 1000 cm<sup>-1</sup> due to ring breathing modes of aromatic moieties, both in-phase increasing upon perturbation, and the 1003 cm<sup>-1</sup> response is followed by the 1000 cm<sup>-1</sup> band (Figure 2A3"). For non-self-healable p(Sty/nBA) 60:40 copolymers, in-phase responses of the 997 and 1003 cm<sup>-1</sup> bands are detected (Figure 2A4'), and the 1003 cm<sup>-1</sup> response is followed by the 997 cm<sup>-1</sup> band (Figure 2A4"). These data are complemented by deconvoluting the 1000 cm<sup>-1</sup> band into three bands (Figure S12) as well as predicting Raman shift intensities from MD simulations (VAMP module) for off-centered/T-shaped, unperturbed, and face-centered Sty-Sty interactions.<sup>24</sup> The highest intensities (Au) are observed for face-centered (1003 cm<sup>-1</sup>), uninterrupted (1000 cm<sup>-1</sup>), and off-centered parallel/Tshaped (997 cm<sup>-1</sup>) rings (Figure S13). The 2D-COS Raman spectra analysis summary is depicted in Figure 2A5,A6 for selfhealable (interchain face-centered/unperturbed Sty) and nonself-healable (off-centered/intrachain face-centered Sty) copolymers. Although even uninterpreted styrene on p(Sty/nBA)is expected to have asymmetry represented by splitting the C-C breathing mode, recent studies have shown that even free benzene rings exhibit no even potential energy surfaces<sup>25</sup> due to the displacement of H atoms along the in-plane symmetric and out-of-plane bending modes. Although the presence of the 997, 1000, and 1003 cm<sup>-1</sup> bands may be attributed to off-

centered/T-shaped, unperturbed, and face-centered Sty-Sty interactions,<sup>24</sup> the proximity of nBA side groups containing polar C=O and C-O-C moieties may also play a role. Figure 2B1-B4 illustrates FTIR spectra in the 1600-1800 and 1070-1250 cm<sup>-1</sup> regions and the corresponding 2D-COS SYN and ASYN analysis in Figure 2B1'-B4' and B1"-B4", respectively. The responses of the 1158 and 1145 cm<sup>-1</sup> bands are in-phase but in opposite directions (Figure 2B1'; SYN: blue) and initiated by the C-O groups at 1145 cm<sup>-1</sup> (Figure 2B1"; ASYN: red). On the other hand, the C=O and H-bonded C=O groups respond in-phase in opposite directions (1728 and 1716 cm<sup>-1</sup>, respectively) (Figure 2B2'; SYN: blue) and the H-bonded C=O groups respond first (Figure 2B2"; ASYN: red). Thus, C=O and H-bonded C=O groups respond sequentially to damage-repair, which parallels the responses of Sty rings and conformational changes around C-O-C moieties.

Since relatively narrow copolymer molar ratios (45:55–53:47) facilitate self-healing (55:45 molar ratios do not self-heal), we calculated cohesive energies (CE) for model dodecade sequences composed of Sty and nBA units using theoretical and experimental reactivity ratios as input. Conducted under NVT MD equilibration conditions (Supporting Material), Figure 3A–D illustrates copolymer topologies of chains extracted from MD simulations and their respective cohesive energy (CE<sub>p</sub>) values for the following  $r_s$  and  $r_b$  reactivity ratios: A:  $r_s = r_b = 5$ ; B:  $r_s = r_b = 1$ ; C:  $r_s = 0.88$  and  $r_b = 0.22$ ; and D:  $r_s = r_b = 0$ .

The highest  $CE_p$  values (3413.4 kJ/mol) are for purely alternating pairs (D), whereas predominately blocked topologies exhibit the lowest values (3313.6 kJ/mol), again implying (Figure 1) that the alternating Sty/nBA monomer sequences favor overall higher  $CE_p$  and self-healing (Figure 1A). Furthermore, viscoelastic length transitions (VLTs) obtained in DMA experiments show that the junction densities  $(\nu j)$  due to chain entanglements of adjacent chains as well as stored entropy during damage are the highest for self-healable copolymers (Figure 3C and Table S8).

During the damage—repair cycle, the displacement of macromolecular chains causes chain compression near the damaged region. To simulate this effect, we independently pressurized each p(Sty/nBA) cell composed of 47:53 (Figure 4A1,A2), 40:60 (B1,B2), and 60:40 (C1,C2) from 0 to 200

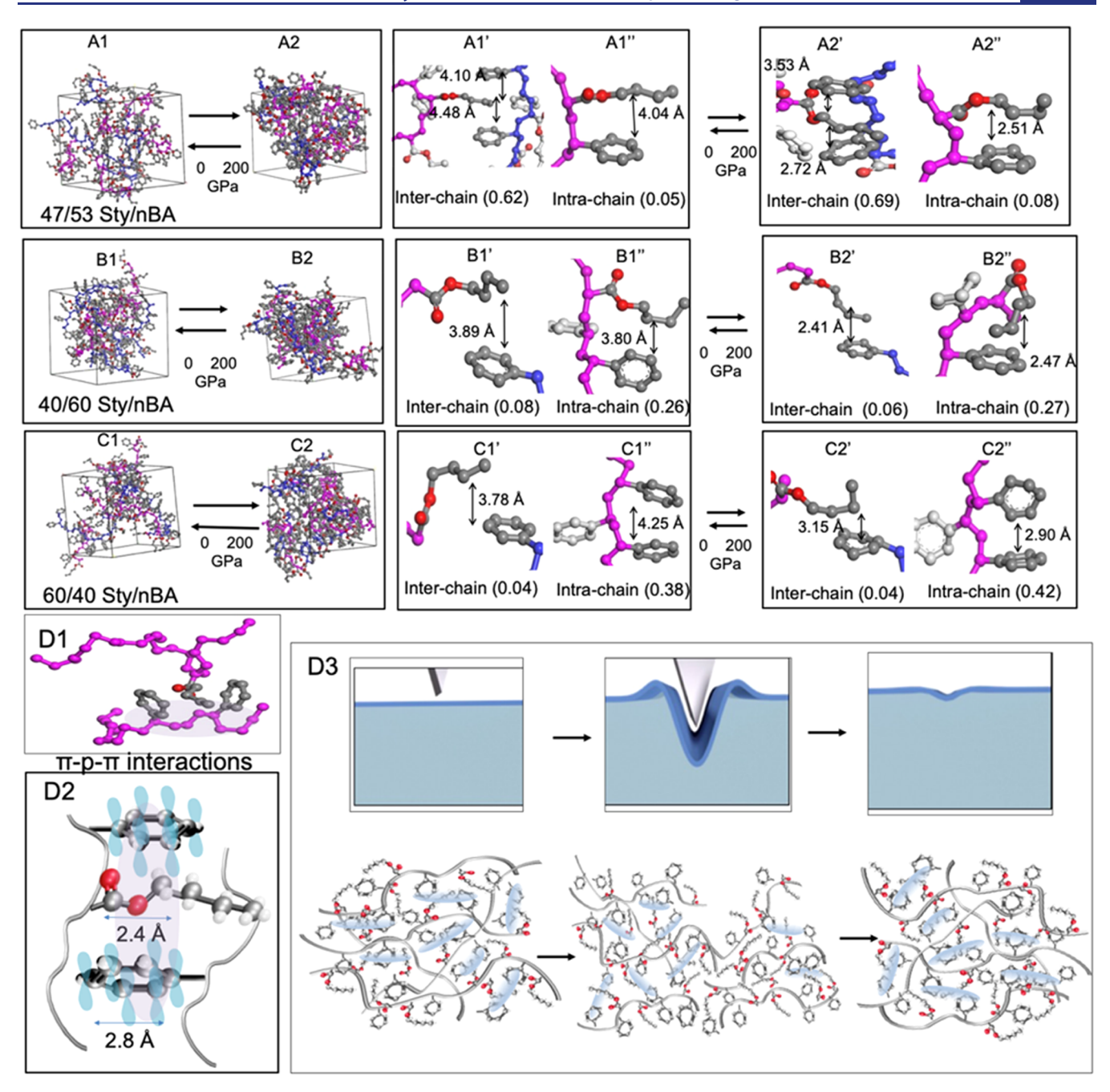


Figure 4. Molecular dynamics simulations under pressure. A series of MD simulations (A–C) for copolymer cells with experimental reactivity ratios of  $r_{\rm s}=0.88$  and  $r_{\rm b}=0.2221$  composed on monomer molar ratios: 47:53 (A series), 40:60 (B series), and 60:40 (C series) pressurized at 0 (A1–C1) and 200 GPa (A2–C2). A1'/A1", B1'/B1", and C1'/C1" and A2'/A2", B2'/B2", and C2'/B2" are extracted dominating structural features extracted from A1/A2, B1/B2, and C1/C2 cells. (D1) Prevailing nBA—Sty interactions extracted from self-healable compositions (A1). (D2)  $\pi$ – $\sigma$ - $\pi$  directional interchain interactions between Sty orbitals and polar C–O–C groups of nBA. (D3) Proposed mechanism of p(Sty/nBA) copolymers self-healing achieved by the ring-and-key interchain interactions driven by  $\pi$ – $\sigma$ - $\pi$  interactions.

GPa and determined the fractions of prevailing inter- and intrachain interactions for each topology as well as the distances before and after compression. Although overall distances are diminished upon compression, they return to the original values upon pressure release. However, what is remarkable is the highest fraction (~0.6–0.7) of interchain interactions between *n*BA groups sandwiched by two aromatic rings for self-healable (II—47:53) compositions (Figure 4A1'-A2). On the other hand, intrachain interactions represent only a small fraction (0.05–0.08) of the total interactions (Figure 4A1"-A2"). In contrast, for 40:60 and

60:40 non-self-healable copolymer compositions, only small fractions ( $\sim$ 0.06-0.08 and 0.04, respectively) of interchain interactions are observed (Figure 4B1'-B2' and C1-C2") and the higher fractions are represented by intrachain interactions (0.26-0.27 and 0.38-0.42, respectively) (Table S9).

If indeed *n*BA side chains are sandwiched between aromatic groups forming *ring-and-lock* interchain interactions facilitating self-healing, the electronic structure of aromatic rings will be disrupted, which is reflected in the presence of three Raman bands attributed to aromatic rings (Figure 2A). The parallel sensitivity of the C-O-C ether linkages to the damage-repair

cycle also indicates that this polar component of aliphatic nBA side groups forms pi—sigma—pi  $(\pi-\sigma-\pi)$  interactions through the oxygen lone pair  $(O_{lp})$ , which stabilize  $\pi$  aromatic rings. Notably, the C–O–C linkages are known to be sensitive to compressive forces, and the electronic interactions between these butyl groups and nonpolar aromatic rings have been only identified for selected biological systems. <sup>27</sup> In contrast to nonself-healable compositions (regions I and III, Figure 1A), aliphatic polar components of nBA-nBA and aromatic  $\pi-\pi$  interactions in the absence of sufficient interchain interactions prevent the chains from recovering and do not self-heal.

Analysis of spectroscopic data and MD simulations show that dipolar aliphatic CH<sub>alkvl</sub> ends are not sensitive to the damage-repair cycle and most likely do not participate in selfhealing. However, their flexibility and mobility may favor the local accessibility of free volume, enabling other rearrangements. Specifically, the polar C-O-C ether group through the  $O_{lp}$  may form energetically favorable  $\pi - \sigma - \pi$  directional interactions. Figure 4D1 shows an example of these interactions extracted from MD simulations for self-healable Sty/nBA monomer molar ratios (region I, Figure 1A), whereas Figure 4D2 illustrates that the approximate lengths of overlapping polar C-O-C segments and Sty rings are approximately 2.4 and 2.8 Å, respectively. Notably, these molecular overlaps are in the ~3 Å range for biological systems.<sup>28</sup> Considering common differences between aromatic groups with high polarizability (hydrophobicity) and localized polarity (hydrophilicity of C-O-C) on nBA, one could argue that preferentially alternating topologies favor intrachain interactions (Figure 4A1"-A2"). On the contrary, these studies show that interchain  $\pi - \sigma - \pi$  interactions prevail for self-healable copolymer compositions reflected in the experimentally determined highest radius of gyration  $(r_g)$  values (Table S1) and end-to-end distances (req) predicted by MD simulations (Figure 1A). The effect of controllable hydrophilicity by externally introduced confined water molecules in the vicinity of hydrophobic moieties has also shown accelerated self-healing.<sup>29</sup> To achieve self-healable p(Sty/ nBA), the internal localized hydrophilic-hydrophobic balance will be critical.

In summary, interchain  $\pi - \sigma - \pi$  interactions recognized as the reoccurring binding elements in proteins, nucleic acids, lipids, or polysaccharides, as well as molecular recognition sites, may offer stabilization of three-dimensional (3D) macromolecular synthetic architectures upon mechanical damage. These weak and largely unexploited ubiquitous van der Waals forces between soft acid aliphatic and soft base aromatic components are largely underutilized in synthetic materials. The ability of styrene-based commodity copolymers to self-heal by forming ring-and-lock interactions may positively impact materials' sustainability challenges, increasing safety by maintaining functionality and preserving from environmental contamination.

## ASSOCIATED CONTENT

# Supporting Information

The Supporting Information is available free of charge at https://pubs.acs.org/doi/10.1021/jacs.3c01199.

Experimental methods; materials; supporting data;  $^1H$  NMR spectrum of the 40:60 p(Sty/nBA) copolymer; GPC chromatograms; DSC curve of p(Sty-b-nBA) copolymers in the temperature range of -100 to +150

°C; glass-transition temperature ( $T_g$ ) and the actual molar ratio of p(Sty/nBA) copolymers; and percent fractions of inter- and intrachain interactions determined from MD simulations (PDF)

Self-healing video p(Sty-nBA) (ZIP)

#### AUTHOR INFORMATION

#### **Corresponding Author**

Marek W. Urban — Department of Materials Science and Engineering, Clemson University, Clemson, South Carolina 29634, United States; orcid.org/0000-0002-1522-2736; Email: mareku@clemson.edu

### **Author**

Samruddhi Gaikwad — Department of Materials Science and Engineering, Clemson University, Clemson, South Carolina 29634, United States

Complete contact information is available at: https://pubs.acs.org/10.1021/jacs.3c01199

#### **Author Contributions**

All authors have given approval to the final version of the manuscript.

#### **Funding**

This work was supported by the National Science Foundation under Award DMR 2003005 and partially by the J.E. Sirrine Foundation Endowment at Clemson University.

#### **Notes**

The authors declare no competing financial interest.

## ACKNOWLEDGMENTS

The authors thank K. Ivey for technical assistance in DSC and DMA measurements.

#### REFERENCES

- (1) Bockstaller, M. R.; Thomas, E. L. Optical properties of polymer-based photonic nanocomposite materials. *J. Phys. Chem. B* **2003**, *107*, 10017–10024.
- (2) Wu, X.; Hou, Q.; Huang, J.; Chai, J.; Zhang, F. Exploring the OH-initiated reactions of styrene in the atmosphere and the role of van der Waals complex. *Chemosphere* **2021**, 282, No. 131004.
- (3) Díaz-de-Mera, Y.; Aranda, A.; Martínez, E.; Rodríguez, A. A.; Rodríguez, D.; Rodriguez, A. Formation of secondary aerosols from the ozonolysis of styrene: effect of SO<sub>2</sub> and H<sub>2</sub>O. *Atmos. Environ.* **2017**, *171*, 25–31.
- (4) Wang, S.; Urban, M. W. Self-healing polymers. *Nat. Rev. Mater.* **2020**, *5*, 562–583.
- (5) Chen, X.; Dam, M. A.; Ono, K.; Mal, A.; Shen, H.; Nutt, S. R.; Sheran, K.; Wudl, F. A Thermally Re-mendable Cross-Linked Polymeric Material. *Science* **2002**, *295*, 1698–1702.
- (6) Yang, Y.; Urban, M. W. Self-Repairable Polyurethane Networks by Atmospheric Carbon Dioxide and Water. *Angew. Chem., Int. Ed.* **2014**, *53*, 12142–12147.
- (7) Ghosh, B.; Urban, M. W. Self-repairing oxetane-substituted chitosan polyurethane networks. *Science* **2009**, 323, 1458–1460.
- (8) Cordier, P.; Tournilhac, F.; Soulié-Ziakovic, C.; Leibler, L. Selfhealing and thermoreversible rubber from supramolecular assembly. *Nature* **2008**, *451*, 977–980.
- (9) Yan, X.; Liu, Z.; Zhang, Q.; Lopez, J.; Wang, H.; Wu, H.-C.; Niu, S.; Yan, H.; Wang, S.; Lei, T.; et al. Quadruple H-bonding cross-linked supramolecular polymeric materials as substrates for stretchable, antitearing, and self-healable thin film electrodes. *J. Am. Chem. Soc.* 2018, 140, 5280–5289.
- (10) Holten-Andersen, N.; Harrington, M. J.; Birkedal, H.; Lee, B. P.; Messersmith, P. B.; Lee, K. Y. C.; Waite, J. H. pH-induced metal-

- ligand cross-links inspired by mussel yield self-healing polymer networks with near-covalent elastic moduli. *Proc. Natl. Acad. Sci. U.S.A.* **2011**, *108*, 2651–2655.
- (11) Urban, M. W.; Davydovich, D.; Yang, Y.; Demir, T.; Zhang, Y.; Casabianca, L. Key-and-lock commodity self-healing copolymers. *Science* **2018**, *362*, 220–225.
- (12) Cao, Y.; Morrissey, T. G.; Acome, E.; Allec, S. I.; Wong, B. M.; Keplinger, C.; Wang, C. A transparent, self-healing, highly stretchable ionic conductor. *Adv. Mater.* **2017**, *29*, No. 1605099.
- (13) White, S. R.; Sottos, N.; Geubelle, P.; Moore, J.; Kessler, M. R.; Sriram, S.; Brown, E.; Viswanathan, S. Autonomic healing of polymer composites. *Nature* **2001**, *409*, 794–797.
- (14) Corten, C. C.; Urban, M. W. Repairing polymers using oscillating magnetic field. *Adv. Mater.* **2009**, *21*, 5011–5015.
- (15) Liu, Q.; Wang, S.; Zhao, Z.; Tong, J.; Urban, M. W. Electrically Accelerated Self-Healable Polyionic Liquid Copolymers. *Small* **2022**, *18*, No. 2201952.
- (16) Wang, S.; Urban, M. W. Self-Healable Fluorinated Copolymers Governed by Dipolar Interactions. *Adv. Sci.* **2021**, *8*, No. 2101399.
- (17) Wang, S.; Li, L.; Liu, Q.; Urban, M. W. Self-healable acrylic-based covalently adaptable networks. *Macromolecules* **2022**, *55*, 4703–4709.
- (18) Parkatzidis, K.; Wang, H. S.; Truong, N. P.; Anastasaki, A. Recent developments and future challenges in controlled radical polymerization: a 2020 update. *Chem* **2020**, *6*, 1575–1588.
- (19) Sosnowski, S.; Szymanski, R.; Lorandi, F.; Olszewski, M.; Sobieski, J.; Yin, R.; Bockstaller, M. R.; Matyjaszewski, K. Distribution of Alternating Sequences in Methyl Methacrylate/n-Butyl Acrylate Copolymers Prepared by Atom Transfer Radical Polymerization. *Macromolecules* **2021**, *54*, 9837–9849.
- (20) Yin, R.; Zhao, Y.; Gorczyński, A.; Szczepaniak, G.; Sun, M.; Fu, L.; Kim, K.; Wu, H.; Bockstaller, M. R.; Matyjaszewski, K. Alternating Methyl Methacrylate/n-Butyl Acrylate Copolymer Prepared by Atom Transfer Radical Polymerization. *ACS Macro Lett.* **2022**, *11*, 1217–1223.
- (21) Arehart, S. V.; Matyjaszewski, K. Atom transfer radical copolymerization of styrene and n-butyl acrylate. *Macromolecules* 1999, 32, 2221–2231.
- (22) Otts, D. B.; Zhang, P.; Urban, M. W. High fidelity surface chemical imaging at 1000 nm levels: internal reflection IR imaging (IRIRI) approach. *Langmuir* **2002**, *18*, 6473–6477.
- (23) Lasch, P.; Noda, I. Two-dimensional correlation spectroscopy (2D-COS) for analysis of spatially resolved vibrational spectra. *Appl. Spectrosc.* **2019**, *73*, 359–379.
- (24) Martinez, C. R.; Iverson, B. L. Rethinking the term "pistacking". Chem. Sci. 2012, 3, 2191–2201.
- (25) Heo, I.; Lee, J. C.; Ozer, B. R.; Schultz, T. Mass-Correlated High-Resolution Spectra and the Structure of Benzene. *J. Phys. Chem. Lett.* **2022**, *13*, 8278–8283.
- (26) Hornat, C. C.; Yang, Y.; Urban, M. W. Quantitative predictions of shape-memory effects in polymers. *Adv. Mater.* **2017**, 29, No. 1603334.
- (27) Nishio, M.; Umezawa, Y.; Fantini, J.; Weiss, M. S.; Chakrabarti, P.  $CH-\pi$  hydrogen bonds in biological macromolecules. *Phys. Chem. Chem. Phys.* **2014**, *16*, 12648–12683.
- (28) Brandl, M.; Weiss, M. S.; Jabs, A.; Sühnel, J.; Hilgenfeld, R. CH.  $\pi$ -interactions in proteins. *J. Mol. Biol.* **2001**, 307, 357–377.
- (29) Davydovich, D.; Urban, M. W. Water accelerated self-healing of hydrophobic copolymers. *Nat. Commun.* **2020**, *11*, No. 5743.

#### NOTE ADDED AFTER ASAP PUBLICATION

The version of this paper that was published ASAP April 17, 2023, was missing panels A5 and A6 in Figure 2. This error was corrected, and the paper was reposted April 18, 2023.